Cycle Ambiguity Reacquisition in UAV Applications Using a Novel GPS/INS Integration Algorithm

Steven E. Langel, Samer M. Khanafseh, Fang-Cheng Chan, and Boris S. Pervan
Illinois Institute of Technology, Chicago, IL

BIOGRAPHY

Steven Langel is a PhD candidate at the Illinois Institute of Technology. His work focuses on the design of high accuracy, high integrity navigation algorithms for aerospace applications. His work also focuses on the integration of inertial navigation systems with GPS. Steven received his B.S degree in aerospace and mechanical engineering from the Illinois Institute of Technology.

Samer Khanafseh is a research associate at the Illinois Institute of Technology whose work involves high accuracy and high integrity navigation system design. In addition, he performs fundamental research in the field of cycle ambiguity resolution with constrained integrity. Dr. Khanafseh received his PhD degree in mechanical and aerospace engineering from the Illinois Institute of Technology.

Fang-Cheng Chan is a research associate at the Illinois Institute of Technology. His work focuses on designing navigation algorithms for high integrity situations such as precision approach and landing. He also performs research in the field of GPS/INS integration with emphasis on developing new approaches to tightly coupled integration. Dr. Chan received his PhD degree from the Illinois Institute of Technology.

Boris Pervan is an associate professor of aerospace engineering at the Illinois Institute of Technology. His work pervades many fields of navigation research including: carrier phase DGPS, aircraft precision approach and landing, optimal and robust navigation system design, integrity monitoring and integration of inertial and laser sensors with GPS. Dr. Pervan received his PhD degree in aeronautics and astronautics from Stanford University.

ABSTRACT

A novel GPS/INS integration algorithm that is adaptable to high satellite blockage environments is developed. Aviation applications such as autonomous shipboard landing require high degrees of accuracy and integrity which warrants the use of a carrier phase differential GPS navigation architecture. In order to achieve the high positioning accuracy achievable with the carrier phase, it is necessary to resolve the integer cycle ambiguity. To include satellites that are acquired (or lost and reacquired) after the initial fix, a 'dual-track' fixing method is introduced. In this algorithm an independent fixing track is implemented in which constrained-integrity fixes are continuously attempted with the newly acquired satellites.

The performance of the dual track fixing algorithm is further enhanced by the integration of an inertial navigation system (INS) with the GPS carrier phase. In qualitative terms, during brief satellite outages the accurate position propagation provided from the output of the INS will translate into knowledge of the cycle ambiguities for the reacquired satellite. In this work, the integration concept is implemented in a novel GPS/INS mechanization that combines GPS and INS states (including cycle ambiguity states) in one centralized Kalman filter. A covariance analysis of the integrated architecture is carried out for the autonomous shipboard landing application, and the findings are expressed in terms of availability. The result of this work is a navigation architecture capable of providing instrument landing support for a Case-I approach; a feat as yet unrealized.

INTRODUCTION

The problem of shipboard landing using the Global Positioning System (GPS) has been an active area of research over the past decade. For instance, different carrier phase differential GPS (CPDGPS) navigation

architectures for shipboard landing of aircraft have been described in [1], [2] and [3]. A key feature of the dual frequency algorithm described in [1] is its use of geometry-free filtering for cycle estimation of widelane integers. As the approach is initiated, this prior knowledge is used together with the available satellite geometric redundancy to fix specific linear combinations of L1 and L2 cycle ambiguities with high integrity. Fixing with constrained integrity is performed by means of a partial fixing integer bootstrap process. This algorithm was shown to provide good availability provided that the mission is conducted under clear sky conditions [1].

One drawback of this algorithm is that there is no mechanism to regain lost satellites in the event of brief satellite outages. This issue was addressed in the design of a navigation system for the aerial refueling mission [4]. In this mission, satellite blockage is introduced from the refueling tanker body, which degrades the resulting positioning performance. In order to reacquire lost satellites without jeopardizing system integrity, a dual track fixing algorithm is implemented which continuously attempts constrained-integrity fixes with the newly acquired satellites. The resulting positioning solution is therefore always computed using the best available satellite geometry.

In this work we fuse the concepts of geometry-free pre-filtering with the dual track fixing algorithm and consider the problem of shipboard landing in the presence of satellite blockage. The Case-I recovery is a well established carrier landing approach that is routinely executed by Navy pilots and will serve as the mission profile. During a case-I recovery the aircraft must complete a series of high banking maneuvers which will inevitably result in satellite blockage. We will show that even though we combine the benefits of geometry-free pre-filtering with the satellite recovery capability of the dual track fixing algorithm, a GPS navigation architecture does not result in sufficient system availability.

The performance of the dual track fixing algorithm is further enhanced by the integration of an inertial navigation system (INS) with the GPS carrier phase. In qualitative terms, during brief satellite outages the accurate position propagation provided from the output of the INS will translate into knowledge of the cycle ambiguities for the reacquired satellite. In this work, the integration concept is implemented in a novel GPS/INS mechanization that combines GPS and INS states (including cycle ambiguity states) in one centralized Kalman filter.

Covariance analysis is the primary simulation tool and is used to assess navigation system performance. Subsequent sections will depict performance in terms of availability on an approach-by-approach basis.

CARRIER LANDING PATTERNS

Aircraft carrier recovery patterns flown by Navy pilots are quite different depending on the time of day, prevailing weather conditions and visibility. For example, in adverse weather conditions and during all night flight operations the pilot will conduct a case-III approach, shown in figure 1. Due to the lack of visibility, case-III recoveries are conducted one aircraft at a time using an instrument landing system (ILS). On the other hand if the pilot has good visibility and is returning to the ship during the daytime, then he/she will conduct a Case-I approach, shown in figure 2. The advantage of this flight pattern is that it allows the carrier to recover multiple aircraft during any given landing mission. Providing instrument landing support for a Case-I approach is necessary if Unmanned Aerial Vehicles (UAVs) are incorporated into existing carrier fleets.

There are six phases of flight that the aircraft must complete during a case-I recovery. The pilot first enters a holding pattern (phase 1) until they receive notification from the ship that they are cleared to land. Upon receiving clearance, the pilot breaks out of the holding pattern and descends to ‘initial’; the beginning of the final landing approach (phase 2). A constant altitude fly-by is then conducted (phase 3) followed by a 180 degree turn at a high bank angle (phase 4). Finally, the aircraft proceeds back towards the carrier (phase 5) and completes another 180 degree turn before arriving on the flight deck. It is important to realize that the pilot will be banking during this approach which will ultimately result in satellite blockage.

Since much effort has already been expended in examining the case-III approach, this work will focus on designing a navigation algorithm that can support automatic shipboard landing of UAVs using a case-I approach.

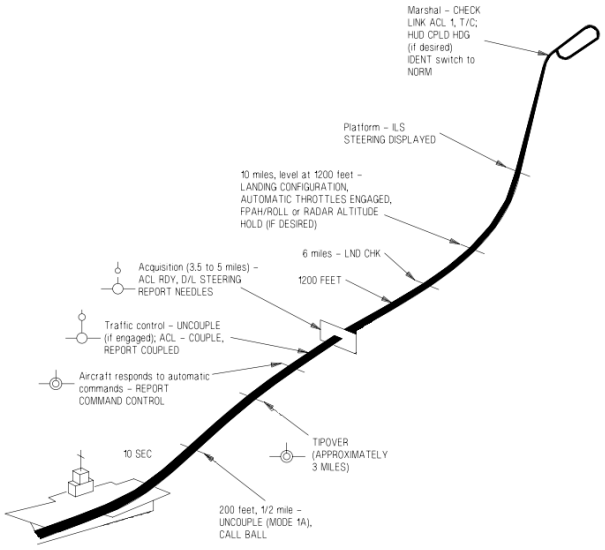

Figure 1: Case-III recovery [10]

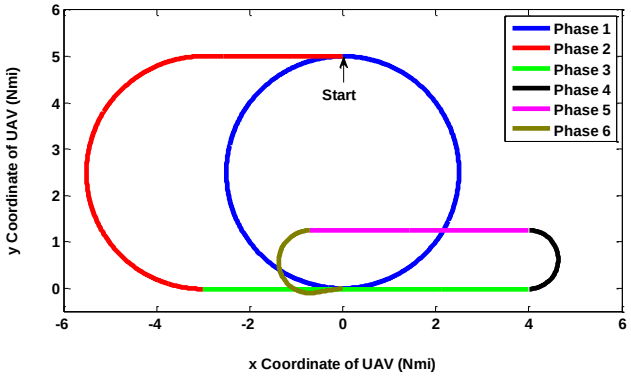

Figure 2: Case-I recovery

BASELINE GPS NAVIGATION ARCHITECTURE

Before describing the end state architecture which includes dual-track fixing and INS, let's first consider the carrier phase differential GPS navigation algorithm depicted in figure 3. This estimation scheme will be the basis of comparison for more elaborate navigation algorithms that will be considered in later sections of this paper. Prior to the initial fix point, the UAV and ship filter the geometry free measurements, z_{GF}. These measurements result in increased observability on individual L1 and L2 cycle ambiguities, which is exploited in one snapshot of geometric redundancy. At this point, specific linear combinations of L1 and L2 integers are fixed with high integrity using the LAMBDA bootstrap method [5]. The output of this process is a partially fixed solution P_k^+ that is fed into a Kalman filter to recursively update the estimation error covariance matrix.

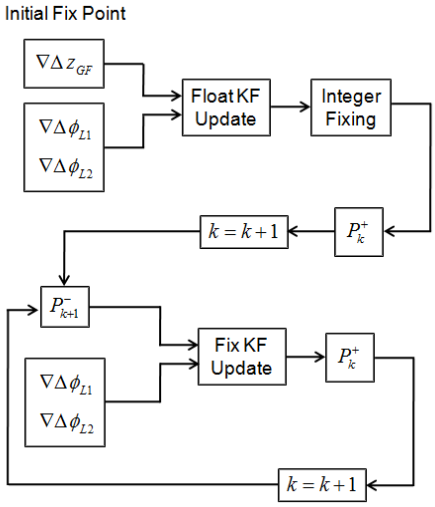

Figure 3: Baseline GPS navigation architecture with geometry-free pre-filtering

In this work, we use the following measurement model for L1 and L2 carrier phase measurements:

$$\phi_{L1} = r + b^s + b_u - I + T + \lambda_{L1}N_{L1} + m_{\phi,L1} + \nu_{\phi,L1} \quad (1)$$

$$\phi_{L2} = r + b^s + b_u - \left(\lambda_{L2}/\lambda_{L1}\right)^2 I + T + \lambda_{L2}N_{L2} + m_{\phi,L2} + \nu_{\phi,L2} \quad (2)$$

Where r is the true range to the satellite, b^s is the satellite clock bias, b_u is the receiver clock bias, I is the ionospheric delay on L1, T is the tropospheric delay, λ_{L1} is the L1 carrier wavelength, N_{L1} is the L1 cycle ambiguity, $m_{\phi,L1}$ is the L1 carrier phase multipath, and $\nu_{\phi,L1}$ is the L1 carrier phase white measurement noise. All terms in equation (2) with an L2 subscript are defined analogously to those given in equation (1).

The satellite clock bias can be eliminated by forming between-receiver single difference measurements for a given satellite.

$$\phi_{ur,L1} = -\hat{\boldsymbol{e}}^T \boldsymbol{x}_{ur} - I_{ur} + T_{ur} + b_{ur} + \lambda_{L1}N_{ur,L1} + m_{\phi,ur,L1} + \nu_{\phi,ur,L1} \quad (3)$$

$$\phi_{ur,L2} = -\hat{\boldsymbol{e}}^T \boldsymbol{x}_{ur} - \left(\lambda_{L2}/\lambda_{L1}\right)^2 I_{ur} + T_{ur} + b_{ur} + \lambda_{L2}N_{ur,L2} + m_{\phi,ur,L2} + \nu_{\phi,ur,L2} \quad (4)$$

Where $(\bullet)_{ur} = (\bullet)_u - (\bullet)_r$ indicates a single difference operation, $\hat{\boldsymbol{e}}$ is the line-of-sight unit vector from the reference receiver to the satellite and $\boldsymbol{x}_{ur}$ is the relative position vector we are trying to estimate.

The differential receiver clock bias b_{ur} can be eliminated by forming between-satellite double difference carrier phase measurements. Denoting the satellite indices as *i* and *j*, the double difference measurement model is given by:

$$\begin{aligned}\nabla\Delta\phi_{L1} = &-\left(\hat{\boldsymbol{e}}^{T,i} - \hat{\boldsymbol{e}}^{T,j}\right)\boldsymbol{x}_{ur} - \left(I_{ur}^{i} - I_{ur}^{j}\right) \\ &+ \left(T_{ur}^{i} - T_{ur}^{j}\right) + \lambda_{L1}\nabla\Delta N_{L1} \\ &+ \left(\Delta m_{L1}^{i} - \Delta m_{L1}^{j}\right) + \nu_{\nabla\Delta\phi,L1}\end{aligned} \tag{5}$$

$$\begin{aligned}\nabla\Delta\phi_{L2} = &-\left(\hat{\boldsymbol{e}}^{T,i} - \hat{\boldsymbol{e}}^{T,j}\right)\boldsymbol{x}_{ur} - \left(\lambda_{L2}/\lambda_{L1}\right)^2\left(I_{ur}^{i} - I_{ur}^{j}\right) \\ &+ \left(T_{ur}^{i} - T_{ur}^{j}\right) + \lambda_{L2}\nabla\Delta N_{L2} \\ &+ \left(\Delta m_{L2}^{i} - \Delta m_{L2}^{j}\right) + \nu_{\nabla\Delta\phi,L2}\end{aligned} \tag{6}$$

Where Δm_{L1} and Δm_{L2} are L1 and L2 single difference multipath states, respectively. In this work, single difference carrier phase multipath is modeled as a first order Gauss Markov random process with an associated time constant, τ. The terms I_{ur} and T_{ur} are the residual ionospheric and tropospheric decorrelation errors, respectively. Provided that the baseline between the user and reference receivers is not too large, these errors are small in comparison to the carrier phase thermal noise. However, as the user-to-reference separation increases, decorrelation errors can no longer be neglected and to do so would jeopardize the robustness of the navigation architecture. Given the baseline distances involved in the case-I recovery shown in figure 2, it is necessary to model the atmospheric decorrelation errors with state augmentation.

There are many models which can be used to estimate the tropospheric delay [11]. Since these corrections are not perfect, some residual error will remain. From the LAAS accuracy models, we have the following expression for the tropospheric decorrelation error [6]:

$$T_{ur} = \frac{10^{-6}\,\Delta n\, h_0}{\sqrt{0.002 + \sin^2\theta}}\left(1 - e^{-\Delta h/h_0}\right) \tag{7}$$

Where Δn is the refractivity index of the troposphere, h_0 is the troposphere scale height (taken to be 7000 m) and Δh is the height of the user above the reference station. All satellites can be included in one tropospheric correction matrix, T. Since the tropospheric decorrelation error model only depends on the refractivity index, the matrix T will be a column vector.

$$\boldsymbol{T} = \begin{bmatrix} T_{ur}^{(1)} - T_{ur}^{(m)} \\ T_{ur}^{(2)} - T_{ur}^{(m)} \\ \vdots \\ T_{ur}^{(n)} - T_{ur}^{(m)} \end{bmatrix} \tag{8}$$

Where $T_{ur}^{(m)}$ is the tropospheric decorrelation error for the master satellite.

For the ionosphere, a model is first imposed for the vertical ionospheric decorrelation error [6]:

$$I_{ur,vert} = vig \cdot \Delta x \tag{9}$$

Where vig is the vertical ionospheric gradient for a given satellite and Δx is the distance between the UAV and ship in the x-direction (see figure 2 for a description of the axes).

The vertical delay given in equation (9) is converted into actual range delay via an obliquity factor [6]:

$$OB_I = \left[1 - \left(\frac{R_e \cos\theta}{R_e + h_I}\right)^2\right]^{-1/2} \tag{10}$$

Where R_e is the earth radius and h_I is the ionospheric shell height (taken to be 350 km). Multiplying the right hand side of equation (9) by the obliquity factor given in equation (10) produces an expression for the ionospheric decorrelation error:

$$I_{ur} = \left[1 - \left(\frac{R_e \cos\theta}{R_e + h_I}\right)^2\right]^{-1/2} \Delta x \cdot vig \tag{11}$$

It is important to note that equation (11) was derived for the LAAS program where the terminal navigation problem involves a straight approach (similar to the case-III approach shown in figure 1). For that landing configuration, ionospheric gradients can only exist in the x-direction. However in the case-I approach, the UAV is separated from the carrier in both the x and y directions

(see figure 2), allowing for ionospheric gradients to exist in two dimensions. To account for this fact, equation (11) is expanded to include two vig states per satellite: vig_x and vig_y.

$$I_{ur} = OB_I \cdot \Delta x \cdot vig_x + OB_I \cdot \Delta y \cdot vig_y \quad (12)$$

Similar to the tropospheric decorrelation error, the residual ionospheric error for all satellites can be placed in one matrix. Recognizing that ionospheric gradients can exist in both the x and y directions, these matrices become:

$$\boldsymbol{I}_{L1}^{x} = \boldsymbol{J}\begin{bmatrix} OB^{(1)} & 0 & \cdots & 0 \\ 0 & OB^{(2)} & \cdots & 0 \\ \vdots & \vdots & \ddots & \vdots \\ 0 & 0 & \cdots & OB^{(n)} \end{bmatrix}\Delta x \quad (13)$$

$$\boldsymbol{I}_{L1}^{y} = \boldsymbol{J}\begin{bmatrix} OB^{(1)} & 0 & \cdots & 0 \\ 0 & OB^{(2)} & \cdots & 0 \\ \vdots & \vdots & \ddots & \vdots \\ 0 & 0 & \cdots & OB^{(n)} \end{bmatrix}\Delta y \quad (14)$$

Where $\boldsymbol{J}$ is the familiar transformation matrix which converts single difference measurements into double difference measurements.

$$\boldsymbol{J} = \begin{bmatrix} 1 & 0 & \cdots & 0 & -1 & 0 & \ldots & 0 & 0 \\ 0 & 1 & \cdots & 0 & -1 & 0 & \cdots & 0 & 0 \\ \vdots & \vdots & \ddots & \vdots & \vdots & \vdots & \ddots & \vdots & \vdots \\ 0 & 0 & \cdots & 1 & -1 & 0 & \cdots & 0 & 0 \\ 0 & \cdots & 0 & 0 & -1 & 1 & 0 & \cdots & 0 \\ 0 & \ldots & 0 & 0 & -1 & 0 & 1 & & 0 \\ \vdots & \ddots & \vdots & \vdots & \vdots & \vdots & \vdots & \ddots & \vdots \\ 0 & \ldots & 0 & 0 & -1 & 0 & 0 & \cdots & 1 \end{bmatrix} \quad (15)$$

Similar expressions exist for the L2 ionospheric decorrelation error.

$$\boldsymbol{I}_{L2}^{x} = \left(\lambda_{L2} \big/ \lambda_{L1}\right)^2 \cdot \boldsymbol{I}_{L1}^{x} \quad (16)$$

$$\boldsymbol{I}_{L2}^{y} = \left(\lambda_{L2} \big/ \lambda_{L1}\right)^2 \cdot \boldsymbol{I}_{L2}^{y} \quad (17)$$

Recall that double difference carrier phase measurements are used for positioning. The model for the range term given in equations (5) and (6) can be written in matrix form for all satellites as:

$$G = J\left[\boldsymbol{e}^{(1)} \quad \boldsymbol{e}^{(2)} \quad \cdots \quad \boldsymbol{e}^{(n)}\right]^T \quad (18)$$

Using equations (8), (13), (14), (15), (16), (17) and (18) the double difference carrier phase measurement model is given by:

$$\begin{bmatrix} \nabla\Delta\boldsymbol{z}_{GF} \\ \nabla\Delta\boldsymbol{\varphi}_{L1} \\ \nabla\Delta\boldsymbol{\varphi}_{L2} \end{bmatrix} = \quad (19)$$

$$\begin{bmatrix} \boldsymbol{0} & \boldsymbol{I} & -\boldsymbol{I} & \boldsymbol{0} & \boldsymbol{0} & \boldsymbol{0} & \boldsymbol{0} & \boldsymbol{0} \\ \boldsymbol{G} & \lambda_{L1}\boldsymbol{I} & \boldsymbol{0} & \boldsymbol{J} & \boldsymbol{0} & \boldsymbol{T} & \boldsymbol{I}_{L1}^{x} & \boldsymbol{I}_{L1}^{y} \\ \boldsymbol{G} & \boldsymbol{0} & \lambda_{L2}\boldsymbol{I} & \boldsymbol{0} & \boldsymbol{J} & \boldsymbol{T} & \boldsymbol{I}_{L2}^{x} & \boldsymbol{I}_{L2}^{y} \end{bmatrix}\boldsymbol{\xi} + \begin{bmatrix} \boldsymbol{v}_{\nabla\Delta z_{GF}} \\ \boldsymbol{v}_{\nabla\Delta\phi,L1} \\ \boldsymbol{v}_{\nabla\Delta\phi,L2} \end{bmatrix}$$

$$\boldsymbol{\xi} = \left[\boldsymbol{x}_{ur} \quad \nabla\Delta\boldsymbol{N}_{L1} \quad \nabla\Delta\boldsymbol{N}_{L2} \quad \Delta\boldsymbol{m}_{L1} \quad \Delta\boldsymbol{m}_{L2} \quad \boldsymbol{\xi}_{atmos}\right]$$

Where $\boldsymbol{\xi}_{atmos}$ is a subset of the state vector corresponding to the atmospheric states Δn, $\boldsymbol{vig}_x$ and $\boldsymbol{vig}_y$.

$$\boldsymbol{\xi}_{atmos} = \left[\Delta n \quad \boldsymbol{vig}_x \quad \boldsymbol{vig}_y\right] \quad (20)$$

Note that the measurement vector given in equation (19) consists of the geometry-free measurement $\nabla\Delta\boldsymbol{z}_{GF}$ and L1 and L2 double difference carrier phase measurements. It is important to realize that $\nabla\Delta\boldsymbol{z}_{GF}$ is only included in the measurement model when the Kalman filter is initialized. After the geometric redundancy snapshot, only carrier phase measurements can be used for relative positioning.

The state transition matrix is given by:

$$\boldsymbol{x}_{GPS,k+1} = \boldsymbol{\Phi}_{GPS}\ \boldsymbol{x}_{GPS,k} + \boldsymbol{w}_{GPS,k} \quad (21)$$

Where $\boldsymbol{x}_{GPS,k}$ is the GPS state vector at time *k* and $\boldsymbol{w}_{GPS,k}$ is the associated process noise at time *k*.

$$\boldsymbol{\Phi}_{GPS} = \begin{bmatrix} \boldsymbol{I} & \boldsymbol{0} & \boldsymbol{0} & \boldsymbol{0} & \boldsymbol{0} & \boldsymbol{0} & \boldsymbol{0} & \boldsymbol{0} \\ \boldsymbol{0} & \boldsymbol{I} & \boldsymbol{0} & \boldsymbol{0} & \boldsymbol{0} & \boldsymbol{0} & \boldsymbol{0} & \boldsymbol{0} \\ \boldsymbol{0} & \boldsymbol{0} & \boldsymbol{I} & \boldsymbol{0} & \boldsymbol{0} & \boldsymbol{0} & \boldsymbol{0} & \boldsymbol{0} \\ \boldsymbol{0} & \boldsymbol{0} & \boldsymbol{0} & e^{-T/\tau}\boldsymbol{I} & \boldsymbol{0} & \boldsymbol{0} & \boldsymbol{0} & \boldsymbol{0} \\ \boldsymbol{0} & \boldsymbol{0} & \boldsymbol{0} & \boldsymbol{0} & \boldsymbol{e}^{-T/\tau}\boldsymbol{I} & \boldsymbol{0} & \boldsymbol{0} & \boldsymbol{0} \\ \boldsymbol{0} & \boldsymbol{0} & \boldsymbol{0} & \boldsymbol{0} & \boldsymbol{0} & 1 & \boldsymbol{0} & \boldsymbol{0} \\ \boldsymbol{0} & \boldsymbol{0} & \boldsymbol{0} & \boldsymbol{0} & \boldsymbol{0} & \boldsymbol{0} & \boldsymbol{I} & \boldsymbol{0} \\ \boldsymbol{0} & \boldsymbol{0} & \boldsymbol{0} & \boldsymbol{0} & \boldsymbol{0} & \boldsymbol{0} & \boldsymbol{0} & \boldsymbol{I} \end{bmatrix} \quad (22)$$

Where T is the sampling time and τ is the time constant associated with the L1 and L2 multipath models. Notice that the state transition matrix assumes all state variables are constant from one time step to the next with the exception of the multipath states. While this model is exact for the integer states and sufficient for the atmospheric states, it is not adequate for the position state. It is obvious that the UAV will move from one measurement epoch to the next, and this is not captured in the dynamic model. In order to account for the lack of a dynamic model for the UAV, we put infinite process noise on the position state. The process noise covariance matrix can therefore be written as:

$$\mathrm{cov}(\boldsymbol{w}_{GPS}) = \quad (23)$$

$$\begin{bmatrix} \infty\boldsymbol{I} & \boldsymbol{0} & \boldsymbol{0} & \boldsymbol{0} & \boldsymbol{0} & \boldsymbol{0} & \boldsymbol{0} & \boldsymbol{0} \\ \boldsymbol{0} & \boldsymbol{0} & \boldsymbol{0} & \boldsymbol{0} & \boldsymbol{0} & \boldsymbol{0} & \boldsymbol{0} & \boldsymbol{0} \\ \boldsymbol{0} & \boldsymbol{0} & \boldsymbol{0} & \boldsymbol{0} & \boldsymbol{0} & \boldsymbol{0} & \boldsymbol{0} & \boldsymbol{0} \\ \boldsymbol{0} & \boldsymbol{0} & \boldsymbol{0} & \sigma^2_{\Delta\varphi}\boldsymbol{I}\left(\boldsymbol{1}-\boldsymbol{e}^{-T/\tau}\right) & \boldsymbol{0} & \boldsymbol{0} & \boldsymbol{0} & \boldsymbol{0} \\ \boldsymbol{0} & \boldsymbol{0} & \boldsymbol{0} & \boldsymbol{0} & \sigma^2_{\Delta\varphi}\boldsymbol{I}\left(\boldsymbol{1}-\boldsymbol{e}^{-T/\tau}\right) & \boldsymbol{0} & \boldsymbol{0} & \boldsymbol{0} \\ \boldsymbol{0} & \boldsymbol{0} & \boldsymbol{0} & \boldsymbol{0} & \boldsymbol{0} & 0 & \boldsymbol{0} & \boldsymbol{0} \\ \boldsymbol{0} & \boldsymbol{0} & \boldsymbol{0} & \boldsymbol{0} & \boldsymbol{0} & \boldsymbol{0} & \boldsymbol{0} & \boldsymbol{0} \\ \boldsymbol{0} & \boldsymbol{0} & \boldsymbol{0} & \boldsymbol{0} & \boldsymbol{0} & \boldsymbol{0} & \boldsymbol{0} & \boldsymbol{0} \end{bmatrix}$$

Where $\sigma_{\Delta\phi}$ is the standard deviation of the single difference carrier phase multipath driver noise.

BASELINE GPS ALGORITHM SIMULATION

The performance of the GPS architecture can be evaluated through a covariance analysis. Parameters used to carry out the simulation are given below in table 1.

Table 1: Simulation parameters

Parameter	Simulation Value
Mission Location	Atlantic Ocean
Satellite Constellation	30 SV almanac
Single difference code sigma ($\sigma_{\Delta\rho}$)	0.5 m
Single difference Carrier sigma ($\sigma_{\Delta\varphi}$)	1 cm
Airframe multipath Time constant (τ_a)	20 sec
Shipboard multipath Time constant (τ_s)	60 sec
Aircraft elevation mask	5 deg
Shipboard elevation mask	7.5 deg
Uncertainty in vertical ionospheric gradient (σ_{vig})	4 mm/km
Uncertainty in refractivity Index ($\sigma_{\Delta n}$)	10
Integrity risk	10^{-7}

The performance of the navigation architecture can be examined for a single approach on the basis of availability. A given approach is said to be available if the accuracy and integrity requirements are satisfied at each point along the approach. For the autonomous shipboard landing application, accuracy and integrity requirements are allowed to vary as a function of distance to touchdown, the logic being that these requirements will become more stringent as the UAV comes closer to completing its mission. As we proceed, a hypothetical example of required vertical positioning performance will be defined as a function of distance to touchdown. This is done because the vertical positioning error is generally what results in an unavailable approaches.

Three factors must be considered when determining where to fix the cycle ambiguities: pre-filtering duration, the dynamic nature of the performance drivers and ionospheric and tropospheric robustness. Of course, we wish to pre-filter as long as possible since this will improve cycle ambiguity resolution. However note that before reaching the initial fix point, the UAV must rely on a floating solution for positioning. Since the performance criteria tighten as the UAV comes closer to landing, there is a point where the floating solution will not satisfy the requirements, rendering the approach unavailable. Lastly, the Kalman filter propagation must be robust to the ionospheric and tropospheric decorrelation error models. If the baseline between the UAV and ship becomes too large, the fidelity in the error models diminishes. In order to accommodate these issues, the fixing point shown in figure 4 was selected. This point is approximately 2

nautical miles away from the ship and represents a good compromise for the issues described above.

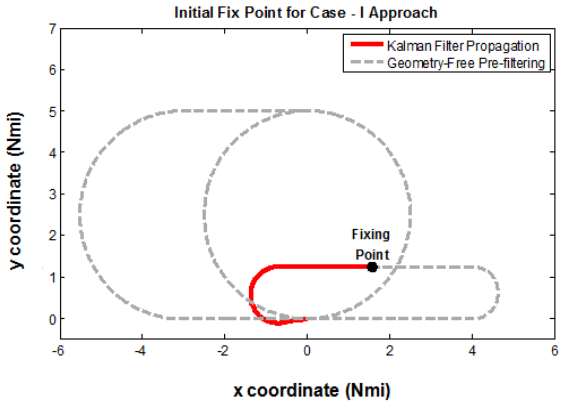

Figure 4: Initial fix point

Using the requirements given in table 1 and the initial fix point shown in figure 4, we can determine the vertical positioning performance for a single approach. Figure 5 depicts the vertical positioning error (σ_v) under various assumptions regarding satellite blockage. The black curve is the actual σ_v that would be observed in the case-I approach. Obviously, this approach would be unavailable since σ_v exceeds the accuracy requirement. However, this case illustrates two interesting effects of the satellite blockage.

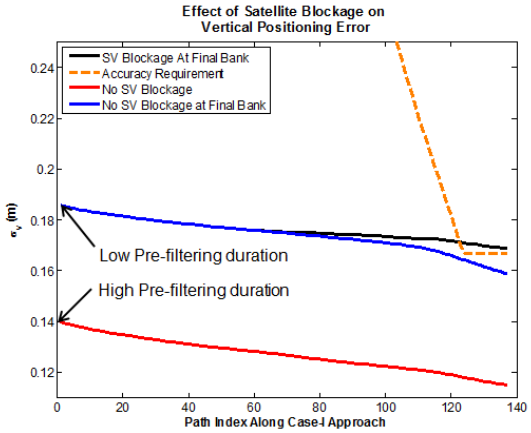

Figure 5: Vertical positioning performance of baseline GPS architecture

Firstly, signal obstruction has an adverse effect on the pre-filtering process. As soon as a satellite is blocked, any pre-filtering information that has been obtained is lost. Consequently, the pre-filtering process must be re-started once that satellite comes back online. The net effect is a reduction in the observability of the L1 and L2 cycle ambiguities, which reduces the number of fixed ambiguities. This is precisely what is observed in figure 5. The red curve plots σ_v assuming that there is no satellite blockage. It is apparent that σ_v starts out with a significantly lower value compared to the black curve, indicating a higher number of fixed ambiguities. Additionally, satellite loss in the final case-I bank leads to a negative impact on vertical position error. The blue curve indicates that the approach would be available if there was no satellite blockage in the final bank. These observations suggest two methods to improve availability. One method to improve availability is to address the pre-filtering limitation. While this is a viable option, it will not be considered in this work. The other option is to address the problem of satellite blockage through the introduction of an inertial navigation system and a "dual-track" fixing algorithm. Each of these approaches will now be discussed individually.

DUAL TRACK FIXING ALGORITHM

The dual track fixing algorithm was developed to contend with satellite blockage for aerial refueling [4]. In this work, we modify the basic structure to take better advantage of the Kalman filter propagation. The basic premise of the dual track fixing algorithm is to continually attempt to fix the current satellite set within the integrity risk requirement. In this way, we ensure the use of the best available satellite geometry for positioning. This algorithm is shown schematically in figure 6.

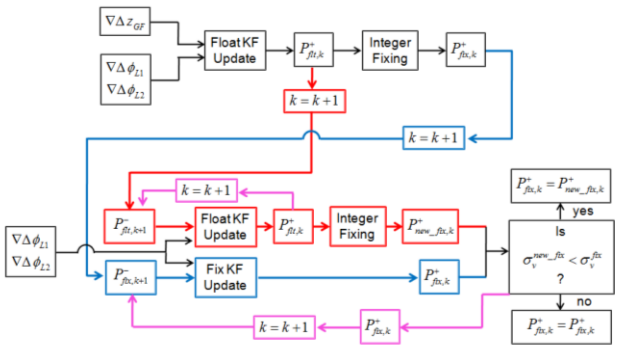

Figure 6: Dual track fixing algorithm

The dual track fixing algorithm begins in the same manner as the baseline GPS navigation architecture shown in figure 3. Pre-filtered widelanes are used with the available carrier phase measurements to execute one geometric redundancy snapshot, resulting in a floating covariance matrix, $P^{+}_{flt,k}$. Integer fixing is conducted next with high integrity which outputs a fixed covariance

matrix, $P^{+}_{fix,k}$. After the initialization step, there are two options. First, a Kalman filter is used to propagate $P^{+}_{flt,k}$ forward and re-execute the integer fixing step, resulting in a new fixed covariance, $P^{+}_{new\_fix,k}$. This is the red track shown in figure 6. The other option is to simply propagate the previously fixed covariance matrix $P^{+}_{fix,k}$ forward using the Kalman filter propagation equations. This is the blue track shown in figure 6. If the vertical positioning error is smaller using the newly fixed covariance, then the primary positioning track will switch to the auxiliary track. If there is no improvement in σ_v, then no switch is made. This process is repeated at each epoch and hence provides a means of recovering blocked satellites. An important issue must be addressed here related to integrity. The integer fixing step is conducted in accordance with a probability of incorrect fix, which is budgeted from the allotted integrity risk. Once the cycle ambiguities have been resolved within the integrity risk, any further fixing will cause an integrity breach. The beauty of the dual track fixing algorithm is that it does not take advantage of any information obtained from prior fixing attempts. Hence, cycle ambiguities are reacquired within the integrity risk requirement.

GPS/INS INTEGRATION

GPS and inertial navigation systems can be coupled using a variety of integration schemes. These can range from the simple loosely coupled integration, to the complex ultra-tightly coupled mode in which the INS directly aids the GPS tracking loops [6]. In this work, we adapt a variant of the tightly coupled integration to the shipboard landing scenario. This integration scheme is attractive because it provides a method to combine GPS and INS states (including cycle ambiguity states) into one centralized Kalman filter [7]. To see how this is done, consider first the fundamental equations of inertial navigation.

For an inertial navigation system, one can derive continuous time dynamic models for the velocity and attitude of the roving vehicle [8]. In state space form, these equations are given by:

$$\begin{bmatrix} {}^{E}\dot{\boldsymbol{v}}_n^{UAV} \\ \dot{\boldsymbol{E}} \end{bmatrix} = \begin{bmatrix} -\left(2\,{}^{I}\boldsymbol{\omega}^{E} + {}^{E}\boldsymbol{\omega}^{N}\right)\times & \boldsymbol{0} \\ -\boldsymbol{F}_{Eu}\,{}^{B}\boldsymbol{R}^{N}\boldsymbol{F}_{v2T} & \boldsymbol{0} \end{bmatrix} \begin{bmatrix} {}^{E}\boldsymbol{v}_n^{UAV} \\ \boldsymbol{E} \end{bmatrix} + \begin{bmatrix} {}^{N}\boldsymbol{R}^{B}\boldsymbol{f} + \boldsymbol{g} \\ \boldsymbol{F}_{Eu}\,{}^{I}\boldsymbol{\omega}^{B} - \boldsymbol{F}_{Eu}\,{}^{B}\boldsymbol{R}^{N}\,{}^{I}\boldsymbol{\omega}^{E} \end{bmatrix} \tag{24}$$

Where ${}^{E}\boldsymbol{v}_n^{UAV}$ is the ground velocity of the UAV, $\boldsymbol{E}$ is the attitude of the UAV (roll, pitch, and yaw), ${}^{I}\boldsymbol{\omega}^{E}$ is the rotation rate of the earth, ${}^{E}\boldsymbol{\omega}^{N}$ is the rotation rate of the UAV navigation frame relative to earth, ${}^{B}\boldsymbol{R}^{N}$ is the transformation matrix from the UAV navigation frame to body frame, $\boldsymbol{f}$ is the specific force measured by the accelerometers, $\boldsymbol{g}$ is the gravity vector, ${}^{I}\boldsymbol{\omega}^{B}$ is the inertial angular velocity of the UAV measured by the gyroscopes, $\boldsymbol{F}_{Eu}$ is the transformation matrix which translates the instantaneous body-to-navigation rotation rate, ${}^{N}\boldsymbol{\omega}^{B}$, into Euler angle rotation rate [9], and $\boldsymbol{F}_{v2T}$ is the matrix which translates the UAV velocity, *v*, into the navigation frame rotation rate, ${}^{E}\boldsymbol{\omega}^{N}$ [8].

In addition to these fundamental INS states, one must also include states which model the gravity vector as well as inertial sensor errors such as scale factor errors and misalignment errors. Adding these states to the dynamic model given in equation (24) results in:

$$\begin{bmatrix} {}^{E}\dot{\boldsymbol{v}}_n^{UAV} \\ \dot{\boldsymbol{E}} \\ \dot{\boldsymbol{b}}_g \\ \dot{\boldsymbol{b}}_a \\ \dot{\boldsymbol{g}}_{gm} \end{bmatrix} = \boldsymbol{F}_{INS} \begin{bmatrix} {}^{E}\boldsymbol{v}_n^{UAV} \\ \boldsymbol{E} \\ \boldsymbol{b}_g \\ \boldsymbol{b}_a \\ \boldsymbol{g}_{gm} \end{bmatrix} + \begin{bmatrix} {}^{N}\boldsymbol{R}^{B}\boldsymbol{f} + \boldsymbol{g} \\ \boldsymbol{F}_{Eu}\left({}^{I}\boldsymbol{\omega}^{B} - {}^{B}\boldsymbol{R}^{N}\,{}^{I}\boldsymbol{\omega}^{E}\right) \\ \boldsymbol{0} \\ \boldsymbol{0} \\ \boldsymbol{0} \end{bmatrix} \tag{25}$$

where the dynamic matrix is defined as [7]:

$$\boldsymbol{F}_{INS} =$$

$$\begin{bmatrix} -\left(2\,{}^{I}\boldsymbol{\omega}^{E} + {}^{E}\boldsymbol{\omega}^{N}\right)\times & \boldsymbol{0} & \boldsymbol{0} & -{}^{N}\boldsymbol{R}^{B} & \boldsymbol{F}_{gm2v} \\ -\boldsymbol{F}_{Eu}\,{}^{B}\boldsymbol{R}^{N}\boldsymbol{F}_{v2T} & \boldsymbol{0} & -\boldsymbol{F}_{Eu} & \boldsymbol{0} & \boldsymbol{0} \\ \boldsymbol{0} & \boldsymbol{0} & -\boldsymbol{I}/\tau_g & \boldsymbol{0} & \boldsymbol{0} \\ \boldsymbol{0} & \boldsymbol{0} & \boldsymbol{0} & -\boldsymbol{I}/\tau_a & \boldsymbol{0} \\ \boldsymbol{0} & \boldsymbol{0} & \boldsymbol{0} & \boldsymbol{0} & -\boldsymbol{I}/\tau_{gm} \end{bmatrix}$$

The states $\boldsymbol{b}_g$ and $\boldsymbol{b}_a$ model the gyroscope and accelerometer random bias and are described by first order Gauss Markov processes with time constants τ_g and τ_a, respectively. In addition, the gravity vector will change in magnitude and direction due to the inhomogeneous mass distribution of the earth. These effects are captured in the state $\boldsymbol{g}_{gm}$, also modeled as first order Gauss Markov with a time constant τ_{gm}.

Notice that equation (25) is a continuous time non-linear dynamic model for an inertial navigation system. For simulation purposes, it is customary to simulate such a system by using a linearized Kalman filter. This involves linearizing equation (25) about some nominal trajectory using either a Taylor series expansion or a perturbation method. The details of this linearization process will not be carried out in detail here, but can be found in [7],[8],[9]. Using a linearized Kalman filter recasts the state estimation problem in terms of estimating deviations of the actual state from the reference trajectory. For example, instead of estimating the UAV ground velocity, ${}^{E}\boldsymbol{v}_n^{UAV}$, one would be estimating the deviation of the UAV velocity from the reference value, $\delta\,{}^{E}\boldsymbol{v}_n^{UAV}$. Hence, the linearized INS equations become:

$$\begin{bmatrix} \delta\,{}^{E}\dot{\boldsymbol{v}}_n^{UAV} \\ \delta\dot{\boldsymbol{E}} \\ \delta\dot{\boldsymbol{b}}_g \\ \delta\dot{\boldsymbol{b}}_a \\ \delta\dot{\boldsymbol{g}}_{gm} \end{bmatrix} = \boldsymbol{F}_{INS,Lin} \begin{bmatrix} \delta\,{}^{E}\boldsymbol{v}_n^{UAV} \\ \delta\boldsymbol{E} \\ \delta\boldsymbol{b}_g \\ \delta\boldsymbol{b}_a \\ \delta\boldsymbol{g}_{gm} \end{bmatrix} + \boldsymbol{W}_{INS} \qquad (26)$$

where the linearized dynamic matrix is defined as:

$$\boldsymbol{F}_{INS,Lin} =$$

$$\begin{bmatrix} \boldsymbol{0} & \boldsymbol{f}\times & \boldsymbol{0} & -{}^{N}\boldsymbol{R}^{B} & \boldsymbol{F}_{gm2v} \\ \boldsymbol{F}_{v2T} & -{}^{I}\boldsymbol{\omega}^{N}\times & {}^{N}\boldsymbol{R}^{B} & \boldsymbol{0} & \boldsymbol{0} \\ \boldsymbol{0} & \boldsymbol{0} & -\boldsymbol{I}/\tau_g & \boldsymbol{0} & \boldsymbol{0} \\ \boldsymbol{0} & \boldsymbol{0} & \boldsymbol{0} & -\boldsymbol{I}/\tau_a & \boldsymbol{0} \\ \boldsymbol{0} & \boldsymbol{0} & \boldsymbol{0} & \boldsymbol{0} & -\boldsymbol{I}/\tau_{gm} \end{bmatrix}$$

The process noise term, $\boldsymbol{W}_{INS}$, is inserted here to factor in random disturbances such as scale factor errors, misalignment errors, and random sensor noise in the accelerometer and gyroscopes. This term can be written as [7]

$$\boldsymbol{W}_{INS} = \begin{bmatrix} {}^{N}\boldsymbol{R}^{B}\left(-\delta\boldsymbol{S}_f^{a}\boldsymbol{f} - \delta\boldsymbol{M}_{is}^{a}\boldsymbol{f} - \boldsymbol{v}_a\right) \\ -{}^{N}\boldsymbol{R}^{B}\left(-\delta\boldsymbol{S}_f^{g}\,{}^{I}\boldsymbol{\omega}^{B} - \delta\boldsymbol{M}_{is}^{g}\,{}^{I}\boldsymbol{\omega}^{B} - \boldsymbol{v}_g\right) \\ \boldsymbol{\eta}_g \\ \boldsymbol{\eta}_a \\ \boldsymbol{\eta}_{gm} \end{bmatrix}$$

where $\delta\boldsymbol{S}_f^{a}$ and $\delta\boldsymbol{S}_f^{g}$ are the scale factor error matrices for the accelerometer and gyroscope, respectively, $\delta\boldsymbol{M}_{is}^{a}$ and $\delta\boldsymbol{M}_{is}^{g}$ are the misalignment matrices associated with the accelerometer and gyroscope, $\boldsymbol{v}_a$ is the random sensor noise in the accelerometer, $\boldsymbol{v}_g$ is the random sensor noise in the gyroscope, and $\boldsymbol{\eta}_g$, $\boldsymbol{\eta}_a$, and $\boldsymbol{\eta}_{gm}$ are the driving white noise processes for the Gauss-Markov models.

INTEGRATION MECHANISM

In order to tie the GPS and INS dynamic models together, a relationship between the position state estimated with GPS and the velocity state estimated with the INS must be derived. This type of integration was first implemented in [7] for a stationary reference station. The shipboard landing scenario is different because the reference station (aircraft carrier) is mobile.

Let the position of the UAV relative to the ship be expressed in the ship local level frame, S.

$$\Delta\boldsymbol{x}_s = \boldsymbol{x}_s^{ship} - \boldsymbol{x}_s^{UAV} \qquad (27)$$

Where $\Delta \boldsymbol{x}_s$ is the relative position vector between the UAV and ship expressed in the S frame, $\boldsymbol{x}_s^{ship}$ is the absolute position of the ship, and $\boldsymbol{x}_s^{UAV}$ is the absolute position of the UAV expressed in the S frame.

Differentiating both sides of equation (27) in the S frame results in:

$$\frac{{}^{S}d\Delta \boldsymbol{x}_s}{dt} = \frac{{}^{S}d\,\boldsymbol{x}_s^{ship}}{dt} - \frac{{}^{S}d\,\boldsymbol{x}_s^{UAV}}{dt} \tag{28}$$

Now expand the right hand side of equation (28) in terms of derivatives in the earth frame, E.

$$\begin{aligned}\frac{{}^{S}d\Delta \boldsymbol{x}_s}{dt} = \frac{{}^{E}d\,\boldsymbol{x}_s^{ship}}{dt} + {}^{E}\boldsymbol{\omega}_s^{S} \times \boldsymbol{x}_s^{ship} \\ - \frac{{}^{E}d\boldsymbol{x}_s^{UAV}}{dt} - {}^{E}\boldsymbol{\omega}_s^{S} \times \boldsymbol{x}_s^{UAV}\end{aligned} \tag{29}$$

Where ${}^{E}\boldsymbol{\omega}_s^{S}$ is the angular velocity of the ship body frame relative to the earth frame.

Using the definition of velocity, we arrive at:

$$\frac{{}^{S}d\Delta \boldsymbol{x}_s}{dt} = {}^{E}\boldsymbol{v}_s^{ship} - {}^{E}\boldsymbol{v}_s^{UAV} + {}^{E}\boldsymbol{\omega}_s^{S} \times \Delta \boldsymbol{x}_s \tag{30}$$

However, the velocity that we estimate from the IMU is the ground velocity of the UAV expressed in the UAV's navigation frame. Therefore, we must use a transformation matrix to transform ${}^{E}\boldsymbol{v}_n^{UAV}$ into ${}^{E}\boldsymbol{v}_s^{UAV}$.

$$\frac{{}^{S}d\Delta \boldsymbol{x}_s}{dt} = {}^{E}\boldsymbol{v}_s^{ship} - {}^{S}\boldsymbol{R}^{A}\,{}^{E}\boldsymbol{v}_a^{UAV} + {}^{E}\boldsymbol{\omega}_s^{S} \times \Delta \boldsymbol{x}_s \tag{31}$$

Where ${}^{S}\boldsymbol{R}^{A}$ is a rotation matrix from the UAV navigation frame to the ship navigation frame.

Before equation (31) can be used in the dynamic model, it must be put in a differential form using the same process as in deriving equation (26). The resulting link between GPS and INS states can be written as:

$$\begin{aligned}\delta \Delta \dot{\boldsymbol{x}}_s = \delta \boldsymbol{v}_s^{ship} - {}^{S}\boldsymbol{R}^{A}\delta \boldsymbol{v}_a^{u} + {}^{E}\boldsymbol{\omega}_s^{ship} \times \delta \Delta \boldsymbol{x}_s \\ - \Delta \boldsymbol{x}_s \times {}^{E}\delta \boldsymbol{\omega}_s^{ship}\end{aligned} \tag{32}$$

In order to incorporate the GPS dynamic model given in equation (22) with the INS dynamic model given in equation (26), it must be put in continuous form. Furthermore, we must only consider the subset of the GPS state transition matrix which corresponds to all states excluding the position state. The reason for this is that equation (32) already provides the dynamic model for the relative position vector. Therefore, the appropriate dynamic model for the GPS states is given by:

$$\boldsymbol{F}_{GPS,Lin} = \begin{bmatrix} \boldsymbol{0} & \boldsymbol{0} & \boldsymbol{0} & \boldsymbol{0} & \boldsymbol{0} & \boldsymbol{0} & \boldsymbol{0} \\ \boldsymbol{0} & \boldsymbol{0} & \boldsymbol{0} & \boldsymbol{0} & \boldsymbol{0} & \boldsymbol{0} & \boldsymbol{0} \\ \boldsymbol{0} & \boldsymbol{0} & -\boldsymbol{I}/\tau & \boldsymbol{0} & \boldsymbol{0} & \boldsymbol{0} & \boldsymbol{0} \\ \boldsymbol{0} & \boldsymbol{0} & \boldsymbol{0} & -\boldsymbol{I}/\tau & \boldsymbol{0} & \boldsymbol{0} & \boldsymbol{0} \\ \boldsymbol{0} & \boldsymbol{0} & \boldsymbol{0} & \boldsymbol{0} & 0 & \boldsymbol{0} & \boldsymbol{0} \\ \boldsymbol{0} & \boldsymbol{0} & \boldsymbol{0} & \boldsymbol{0} & \boldsymbol{0} & \boldsymbol{0} & \boldsymbol{0} \\ \boldsymbol{0} & \boldsymbol{0} & \boldsymbol{0} & \boldsymbol{0} & \boldsymbol{0} & \boldsymbol{0} & \boldsymbol{0} \end{bmatrix} \tag{33}$$

Equations (26), (32) and (33) can be put together in one state space model, given below in equation (34).

$$\begin{aligned}\begin{bmatrix} \dot{\boldsymbol{\eta}}_{INS} \\ \delta \Delta \dot{\boldsymbol{x}}_s \\ \dot{\boldsymbol{\eta}}_{GPS} \end{bmatrix} = \begin{bmatrix} \boldsymbol{F}_{INS,Lin} & \boldsymbol{0} & \boldsymbol{0} \\ \boldsymbol{C} & {}^{E}\boldsymbol{\omega}_s^{ship} \times & \boldsymbol{0} \\ \boldsymbol{0} & \boldsymbol{0} & \boldsymbol{F}_{GPS,Lin} \end{bmatrix} \begin{bmatrix} \boldsymbol{\eta}_{INS} \\ \delta \Delta \boldsymbol{x}_s \\ \boldsymbol{\eta}_{GPS} \end{bmatrix} \\ + \begin{bmatrix} \boldsymbol{W}_{INS} \\ \delta \boldsymbol{v}_s^{ship} - \Delta \boldsymbol{x}_s \times \delta \boldsymbol{\omega}_s^{ship} \\ \boldsymbol{W}_{GPS} \end{bmatrix}\end{aligned} \tag{34}$$

$\boldsymbol{C}$ is a matrix defined as:

$$\boldsymbol{C} = \begin{bmatrix} -{}^{S}\boldsymbol{R}^{A} & \boldsymbol{0} & \boldsymbol{0} & \boldsymbol{0} & \boldsymbol{0} \end{bmatrix} \tag{35}$$

Here $\boldsymbol{\eta}_{INS}$ is the INS state vector given in equation (26) and $\boldsymbol{\eta}_{GPS}$ is the subset of the GPS state vector given in equation (12) which consists of all GPS states excluding the relative position state. It is also worth mentioning that since we are using a linearized Kalman filter, the GPS states must also be written in terms of deviations from the nominal trajectory. However, since the GPS dynamic model is already linear, the structure of the state transition matrix remains unchanged.

Also notice that the process noise term on the relative position state involves knowing distributions for the errors in the ship velocity and ship angular velocity. In this work, we chose to neglect these terms and hence assume there is no process noise on the relative position state.

To summarize, equations (34) and (35) provide an equation for the linearized dynamic model of the GPS/INS integrated architecture. As desired, all GPS and INS states have been put in one state vector which can be estimated using a linearized Kalman filter. Before showing results, note that the measurement model is the same as that given in equation (12) since the only external measurements are the GPS measurements. Hence, we obtain:

$$\begin{bmatrix} \nabla\Delta \boldsymbol{z}_{GF} \\ \nabla\Delta \boldsymbol{\varphi}_{L1} \\ \nabla\Delta \boldsymbol{\varphi}_{L2} \end{bmatrix} = \begin{bmatrix} \boldsymbol{0} & \boldsymbol{H}_{GPS} \end{bmatrix} \begin{bmatrix} \boldsymbol{\xi}_{INS} \\ \boldsymbol{\xi}_{GPS} \end{bmatrix} + \begin{bmatrix} \boldsymbol{v}_{\nabla\Delta z_{GF}} \\ \boldsymbol{v}_{\nabla\Delta\varphi,L1} \\ \boldsymbol{v}_{\nabla\Delta\varphi,L2} \end{bmatrix} \quad (35)$$

Where $\boldsymbol{H}_{GPS}$ is the GPS observation matrix given in equation (12), $\boldsymbol{\xi}_{INS}$ is the INS state vector given in equation (26) and $\boldsymbol{\xi}_{GPS}$ is the GPS state vector given in equation (12).

GPS/INS SIMUATION RESULTS

The GPS/INS algorithm described above is applied to the shipboard landing scenario. Vertical positioning performance is compared under various combinations of GPS, INS and dual track. The results are given below in figure (7) for one approach.

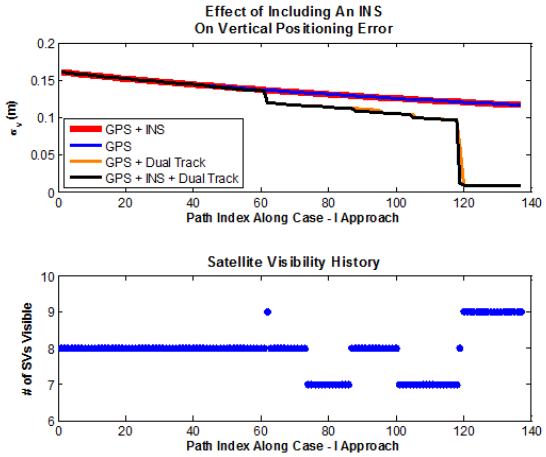

Figure 7: Vertical positioning performance for GPS/INS navigation architecture with satellite visibility history

Notice from figure 7 that the inclusion of INS does not significantly improve the positioning performance for this geometry. However, including the dual track fixing algorithm improves σ_v substantially and it is evident that there is switching taking place. Nevertheless, the same conclusion can be reached with the dual track fixing algorithm: inclusion of the inertial navigation system does not appreciably improve positioning performance.

There are two reasons why the INS does not show improvement for the approach depicted in figure 7. First, the simulation uses a large almanac of 30 SVs. Secondly, the satellite visibility plot given in figure 7 shows that there is not a high degree of satellite blockage. At most, one satellite is lost which drops the number of SVs to 7. With such a high number of satellites, it is reasonable to suspect that the INS will not drastically improve positioning performance for this particular approach. However, all approaches have not been investigated and it is quite possible that the INS will improve positioning performance in these situations. Further study is required and will be conducted in future work.

In order to really observe the benefit of this tightly coupled architecture, consider an application which involves severe sky blockage. For example, this could be an aerial refueling mission or an urban canyon navigation problem. To simulate this, we use the standard do229 almanac [12] and introduce a severe blockage situation.

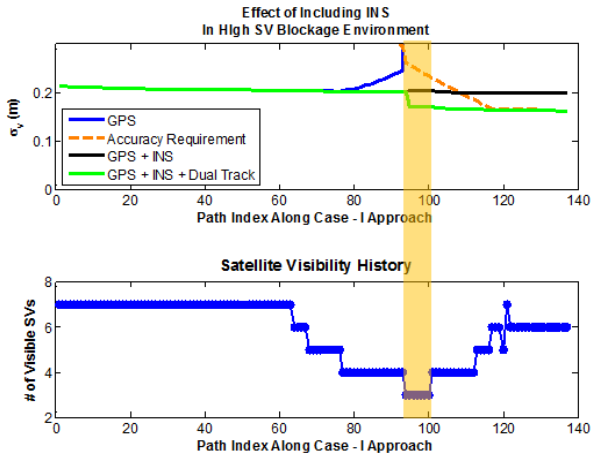

Figure 8: Positioning performance in presence of severe sky blockage with satellite visibility history

Notice from the satellite visibility history plot in figure 8 that the number of visible satellites drops to 3. Therefore, the baseline GPS navigation algorithm will not be able to provide a positioning solution and the approach will be unavailable. Once the INS is included, the navigation system is able to coast through this period of satellite blockage as evidenced by the black curve in figure 8. However, σ_v is still above the accuracy requirement and the approach remains unavailable. The inclusion of the dual track fixing algorithm shows that a switch was made just before dropping to 3 SVs (green curve). From here the INS coasts through the outage and proceeds to the

touchdown point. We can see that in this situation it is the combination of the INS and dual track fixing algorithm which is able to render a previously unavailable approach to an available state.

CONCLUSION

In this work an integrated GPS/INS navigation architecture was developed for the shipboard landing application. Using a novel tightly coupled approach with the dual track fixing algorithm, it was shown for a single landing approach that the INS does not result in a significant improvement in positioning performance. Again it must be restated that this result only applies to a single approach. Future investigation of all approaches will have to be conducted to determine the impact of an inertial navigation system. However, it was shown that this architecture is quite useful in situations with severe satellite blockage. It was shown that the coasting capability of the INS and satellite recovery capability of the dual track algorithm were able to bring a previously unavailable approach to an available state.

ACKNOWLEDGMENTS

We wish to thank our research sponsors who's generous support has allowed us to continue to pursue this research effort.

REFERENCES

[1] M. Heo, B. Pervan, "Carrier Phase Navigation Architecture for Shipboard Relative GPS," IEEE Trans. On Aerospace and Electronic Systems, vol. 42, no. 2, pp. 670-679, April 2006.

[2] S. Dogra, J. Wright, and J. Hansen, "Sea-Based JPALS Relative Navigation algorithm Development," in *Proceedings of the Institute of Navigation 2005 GNSS Meeting*, Long Beach, CA, Sept. 2005.

[3] Petovello, M.G., M.E. Cannon, G. Lachapelle, A. Huang and V. Kubacki (2004), Integration of GPS and INS Using Float Ambiguities with Application to Precise Positioning for JPALS, Proceedings of the ION NTM 2004, San Diego, CA, Jan. 2004.

[4] S. Khanafseh, B. Pervan, and G. Colby, "Carrier Phase DGPS for Autonomous Airborne Refueling," Proceedings of the Institute of Navigation 2005 National Technical Meeting, San Diego, CA, January 24-26, 2004.

[5] P. Teunissen, D. Odijk, and P. Joosten, "A Probabilistic Evaluation of Correct GPS Ambiguity Resolution," Proceedings of the Institute of Navigation's ION GPS-98, Nashville, TN, September 15-18, 1998.

[6] G. A. McGraw, T. Murphy, M. Brenner, S. Pullen, and A. J. Van Dierendonck, "Development of the LAAS Accuracy Models," Proceedings of the Institute of Navigation's ION GPS-2000, Salt Lake City, UT, September 19-22, 2000.

[7] F. C. Chan, "A State Dynamics Method for Integrated GPS/INS Navigation and It's Application To Aircraft Precision Approach," PhD Dissertation, Illinois Institute of Technology, Chicago, IL, May, 2008.

[8] D.H Titterton, J.L. Weston, "Strapdown Inertial Navigation Technology," The American Institute of Aeronautics and Astronautics, 2004.

[9] Jekeli, C., "Inertial Navigation Systems with Geodetic Applications", Berlin, New York, Walter de Gruyter 2001.

[10] Department of the Navy, "NATOPS Flight Manual Navy Model F/A – 18 E/F 165533 And Up Aircraft", March 2001.

[11] *Minimum Operational Performance Standards for Global Positioning System/Wide Area Augmentation System Airborne Equipment*, RTCA Document Number DO-229C, Appendix B.5, Nov. 2001.

[12] P. Misra and P. Enge, *Global Positioning System Signals, Measurements, and Performance*. Lincoln, MA: Ganga-Jumuna Press, 2001.